PROCEEDINGS OF SPIE

SPIEDigitalLibrary.org/conference-proceedings-of-spie

Rotational vibrational-rotational Raman lidar: design and performance of the RASC Raman lidar at Shigaraki, Japan (34.8 degrees N, 136.1 degrees E)

Behrendt, Andreas, Nakamura, Takuji, Sawai, Yukihiko, Onishi, Michitaka, Tsuda, Toshitaka

Andreas Behrendt, Takuji Nakamura, Yukihiko Sawai, Michitaka Onishi, Toshitaka Tsuda, "Rotational vibrational-rotational Raman lidar: design and performance of the RASC Raman lidar at Shigaraki, Japan (34.8 degrees N, 136.1 degrees E)," Proc. SPIE 4484, Lidar Remote Sensing for Industry and Environment Monitoring II, (9 January 2002); doi: 10.1117/12.452774



Event: International Symposium on Optical Science and Technology, 2001, San Diego, CA, United States

Rotational vibrational-rotational Raman lidar: Design and performance of the RASC Raman lidar at Shigaraki (34.8° N, 136.1° E), Japan

Andreas Behrendt*, Takuji Nakamura, Yukihiko Sawai, Michitaka Onishi, Toshitaka Tsuda Radio Science Center for Space and Atmosphere, Kyoto University, Japan

ABSTRACT

The design and the performance of the new Raman lidar of the Radio Science Center for Space and Atmosphere (RASC) at Kyoto University are presented. The system is located at (34.8° N, 136.1° E) near Shigaraki, Japan, where also one of the world largest atmospheric radars, the MU (middle and upper atmosphere) radar, is operated. Measurement parameters of the lidar are atmospheric temperature (with rotational Raman and with Rayleigh integration technique), water vapor mixing ratio (H₂O Raman lidar technique), and optical particle properties. Common Raman lidar takes vibrational-rotational Raman backscatter of nitrogen as a reference signal. In contrast to this, our system makes use of the approximately 10-times stronger pure-rotational Raman signals for deriving both atmospheric temperature and a temperature independent Raman reference signal. This modification leads to a significant reduction of measurement uncertainties. With the RASC lidar, rotational Raman signals with, to our best knowledge, unprecedented intensity can be taken by means of a high-throughput receiver. This allows not only nighttime temperature measurements with a resolution of, e.g., a few minutes near the tropopause, but made also, to our knowledge, the first daytime measurements possible.

Keywords: lidar; laser remote sensing; Raman lidar; rotational Raman lidar; rotational vibrational-rotational Raman lidar; temperature; humidity; aerosols; daytime lidar; cirrus.

1. INTRODUCTION

The Radio Atmospheric Science Center (RASC) of Kyoto University in Uji, Japan, is known for its research in the field of lower, middle, and upper atmosphere dynamics. RASC's main facility for this topic is the MU (middle and upper atmosphere) radar set up in 1984 in Shigaraki. Characteristics of the MU radar are a fast beam steering capability by active phased antennae and a flexible system setup by computer-controlling of the equipment. A large set of instruments for atmospheric observations is operated at the MU radar observatory. Radar systems at the site are a boundary layer radar, a dual-frequency (C/Ku-band) precipitation radar, a UHF boundary layer radar, a lower tropospheric radar, coherent VHF radars for ionosphere observations and the detection of meteor echos, and a millimeter-wave radar for cloud and mist observations. Optical instruments comprise an all-sky airglow imager, a FPI airglow imager (operated by Nagoya University), and a sodium density lidar (operated by Shinshu University). This set of instruments was recently complemented with a combined elastic Raman lidar for the remote profiling of optical particle properties, humidity, and temperature. Here, we introduce the latest stage of this system after a redesign with the implementation of pure-rotational Raman channels and present its first measurements.

This paper contains 6 sections. The introduction is followed by the presentation of a novel technique for deriving a temperature independent reference signal from two pure-rotational Raman signals. Section 3 describes the lidar apparatus. In Section 4 the system performance and the new technique described in Section 2 are illustrated with a measurement example. Measurement data of temperature with rotational Raman technique, of optical particle properties of a cirrus cloud and of moisture are shown and discussed. In section 5, what are to our knowledge the first rotational Raman temperature measurements in daytime are presented. A summary is given in Section 6.

Lidar Remote Sensing for Industry and Environment Monitoring II, Upendra N. Singh, Editor, Proceedings of SPIE Vol. 4484 (2002) © 2002 SPIE · 0277-786X/02/\$15.00

^{*} behrendt@kurasc.kyoto-u.ac.jp; phone +81 774 38 3874; fax +81 774 31 8463; http://www.kurasc.kyoto-u.ac.jp/index-e.html; Radio Science Center for Space and Atmosphere (RASC), Kyoto University, Uji, Kyoto 611-0011, Japan

2. NOVEL TECHNIQUE FOR DERIVING A LIDAR REFERENCE SIGNAL FROM THE PURE-ROTATIONAL RAMAN BACKSCATTERING

Figure 1 shows an overview of lidar backscatter signals and their relative intensities. Common Raman lidar uses the vibrational Raman signal of N_2 or O_2 as reference signal in order to measure independently the atmospheric backscatter coefficient and the extinction coefficient³.

Main advantages of using pure-rotational Raman signals instead of a vibrational Raman signal are the following:

- The intensity of pure-rotational Raman signals is about 10-times higher.
- As the wavelength difference between elastic and rotational Raman reference signal can be neglected, assumptions for the wavelength dependency of the aerosol extinction coefficient are no longer necessary.

Already in the earlier days of lidar it was proposed to use pure-rotational Raman signals for the normalization of elastic lidar returns by extracting parts of the rotational Raman spectrum in such a way that the temperature dependency of this signal is low⁴. The same kind of signal extraction was suggested later for Raman DIAL measurements of ozone concentration⁵. However, the difficulty of extracting a signal which is sufficiently temperature independent over a wider range of temperatures, i.e., especially the lack of control of small misalignments, which might lead to temperature cross-talk of the measurements, is a disadvantage of this technique.

Another way for using a rotational Raman signal as reference signal is to correct for its temperature dependency^{6,7}. In this case, however, uncertainties in the atmospheric temperature profile come to the uncertainty of the exact temperature dependency of the signal.

To overcome these disadvantages, we use the two pure-rotational Raman signals of different temperature dependence not only for atmospheric temperature measurements^{8,9} but also to derive a reference signal which is essentially temperature independent (Figure 2). This is done by calculating the weighted sum of the signals

$$N_{\text{ref}}(z) = N_{\text{RR1}}(z) + c N_{\text{RR2}}(z)$$

with $N_{\rm ref}$ for the reference signal, $N_{\rm RR1}$ and $N_{\rm RR2}$ for the rotational Raman signals, c a constant and z height. The constant c has to be determined by calculating the temperature dependency of the rotational Raman signals taking the spectral characteristics of the receiver into account, but this calculation can be validated experimentally by comparing the calculated with the experimental calibration function used for the temperature measurement. With this method, the relative intensity of the resulting reference signal varies by less than \pm 0.5 % for temperatures between 190 and 260 K (Figure 2c). In cases

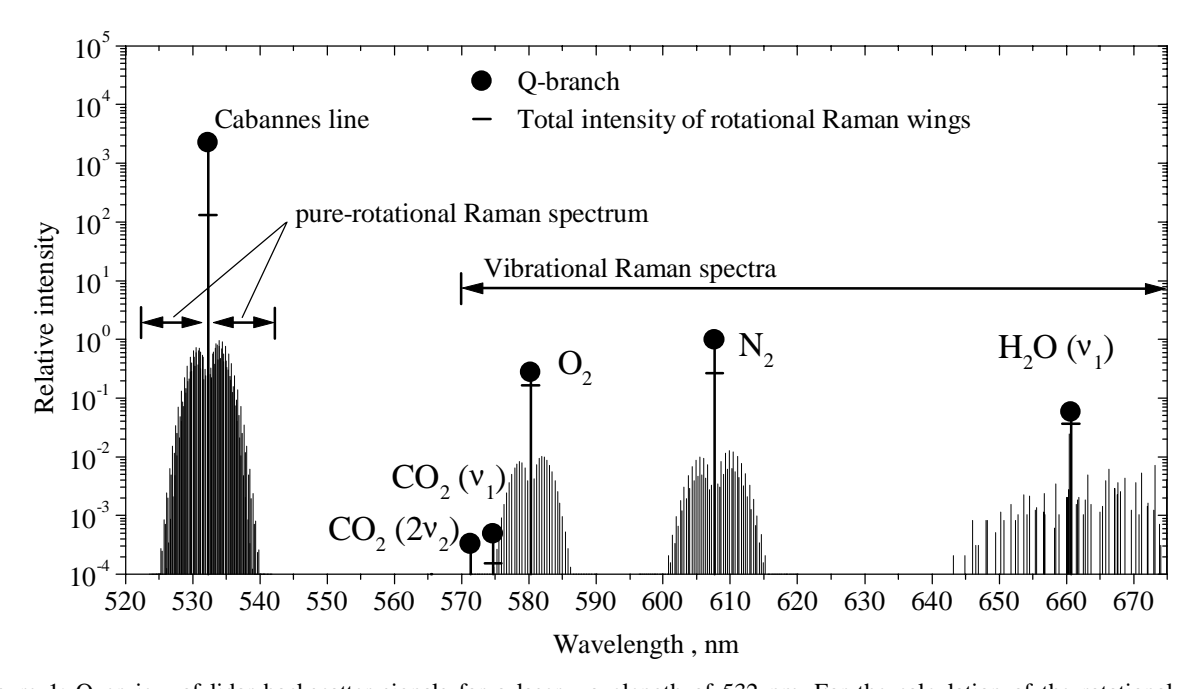
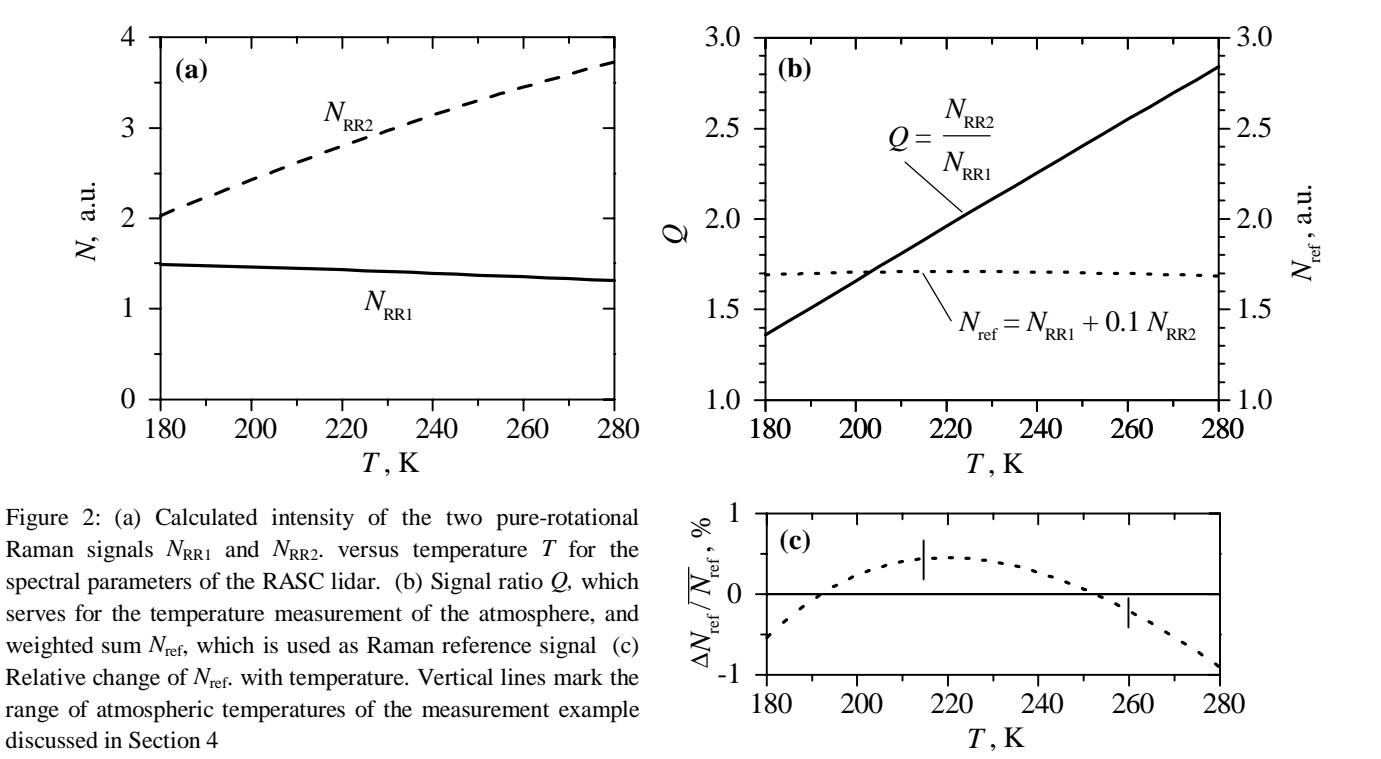


Figure 1: Overview of lidar backscatter signals for a laser wavelength of 532 nm. For the calculation of the rotational wings the temperature was set to 300 K. Atmospheric H_2O mixing ratio was set to 1 %. v_1 and 2 v_2 denote different vibrational modes of the three-atomic molecules H_2O and CO_2 .

where these variations are not negligible compared to the statistical uncertainty of the data, a further correction of the reference signal can be made by fitting the curve in Figure 2c and eliminating even this small dependence with the measured temperature profile.



3. SYSTEM SETUP

A schematic overview over the RASC lidar is shown in Figure 3. The technical data of the system are listed in Table 1. As transmitter, a frequency doubled Nd:YAG laser emitting at 532.11 nm is used. The laser output power is 30 W. The Cassegrain receiving telescope has a primary mirror diameter of 0.82 m.

Figure 4 shows the setup of the dispersion system, a filter polychromator with at present 5 channels. The channels are for the detection of elastic backscattering, pure-rotational Raman signals in two regions of different temperature dependence, and of vibrational Raman signal of water vapor. A fifth channel, which has its own transmitter, is operated by Shinshu University and detects the resonance fluorescence signal of Na atoms in the mesosphere. The optical properties of the components employed for the wavelength separation are given in Table 2. Table 3 summarizes the properties for each receiving channel.

The concept of the RASC lidar for extracting the rotational Raman signals follows a design developed for the Raman lidar of GKSS Research Center, Geesthacht, Germany¹². With the GKSS Raman lidar reliable measurements in clouds became possible by high elastic backscatter suppression for the rotational Raman channels. In addition, high signal extraction efficiency extended the measurement range up to the stratopause region. This allowed to study the formation conditions of polar stratospheric clouds in the Arctic and to compare lidar temperature data measured with Rayleigh integration technique, which has a lower limit of about 30 km height, and rotational Raman technique.^{13,14} This comparison is especially interesting for the study of atmospheric wave phenomena, as the Rayleigh integration technique is based on the assumption that the atmosphere is in hydrostatic equilibrium.

The setup of the RASC lidar contains so far only one channel for the detection of elastic backscattering. As the first measurements with the new system aimed at high performance in the troposphere, neutral density attenuators with a low transmission value were used for the elastic channel, which hindered temperature measurements by Rayleigh integration technique in high altitudes. When this paper was submitted the implementation of a second elastic channel, which will be protected from low-altitude signals by means of a chopper, was already in progress.

For the first measurements of the new RASC lidar, which are presented in Section 4, it was possible to use the narrow-band filters (BS3-BS5) of the GKSS Raman lidar. To compensate for the difference in laser wavelength (532.11 nm instead of 532.25 nm) the angles of incidence of these components were slightly increased so that the extracted portions of the pure-rotational Raman spectrum are the same for both systems.

Table 1: Technical data of the RASC lidar

Laser				
Туре	Frequency-doubled Nd:YAG, injection seeded			
Model	Continuum Powerlite 9050			
Wavelength	532.11 nm			
Pulse energy	600 mJ			
Pulse repetition rate	50 Hz			
Beam divergence	< 500μrad (full angle)			
Transmitter Optics				
Geometry	Galileian telescope			
Expansion factor	8			
Beam divergence of the expanded laser beam	< 60 μrad (full angle)			
Receiver Optics				
Geometry	Cassegrainian telescope			
Primary mirror diameter	820 mm			
Telecope focal length	8000 mm			
Field of view (FOV)	1 mrad (selectable)			
Minimum height of total overlap for above FOV	~ 1200 m			
Dispersion system (further details see Tables 2 and 3)				
Type	5-channel filter polychromator			
Channels	1. Na D ₂ resonance			
	(for collocated Na resonance lidar of Shinshu University)			
	2. H ₂ O vibrational Raman, 1. Stokes			
	3. Elastic backscattering			
	4. Lower quantum number pure-rotational Raman, anti-Stokes5. Higher quantum number pure-rotational Raman, anti-Stokes			
Detectors	unu biokes			
Type	Photomultipliers in single photon counting mode			
Models	Hamamatsu Photonics R943-02, water-cooled (channel 1 and 2)			
Models	Electron Tubes 9863/100 (channel 3)			
	Electron Tubes 9863/350 (channel 4 and 5)			
Discriminators	Electron Tubes AD3			
Data acquisition systems	Election Tubes (195)			
Data adjustition bystoms	EG&G MCS-Plus (channel 2 and 3)			
	Optech FDC-700M (channel 4 and 5)			
	opicen i De 700m (enamer + and 3)			

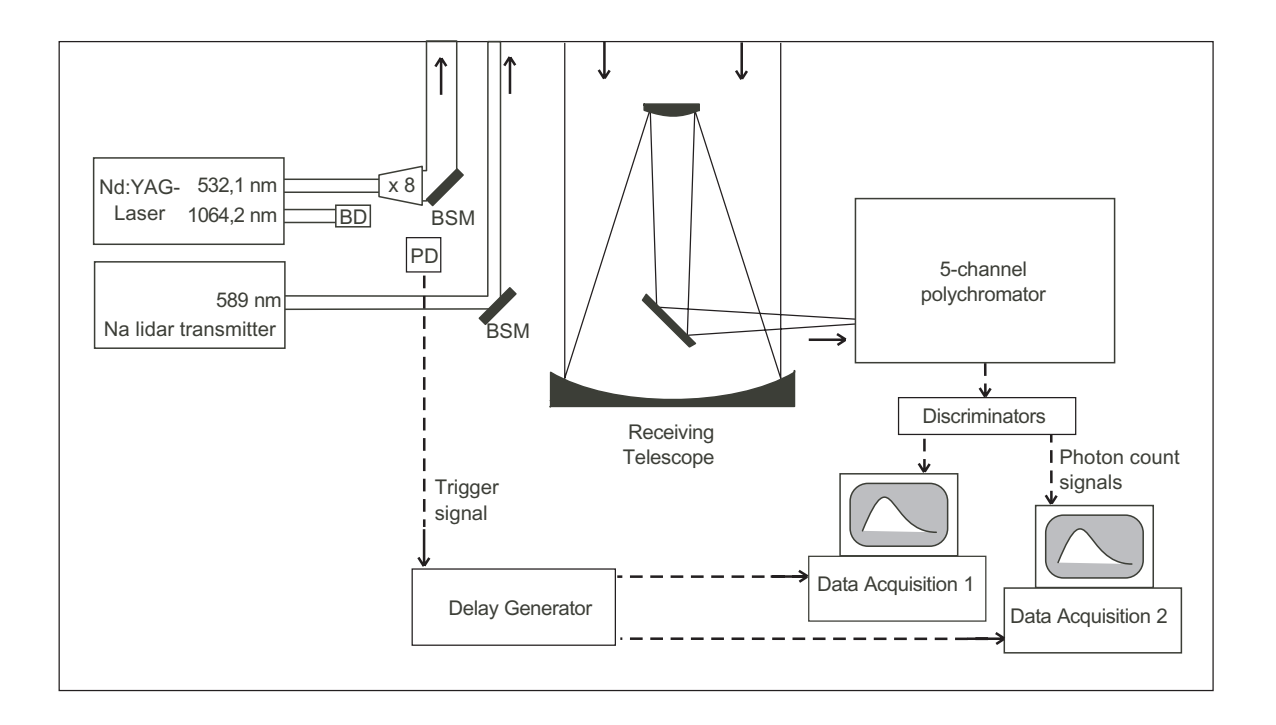


Figure 3: Schematic overview of the RASC lidar setup. BD beam dump, PD photodiode, BSM beam steering mirror. TheNa lidar transmitter serves for a collocated system, whose data acquisition system is not shown here.

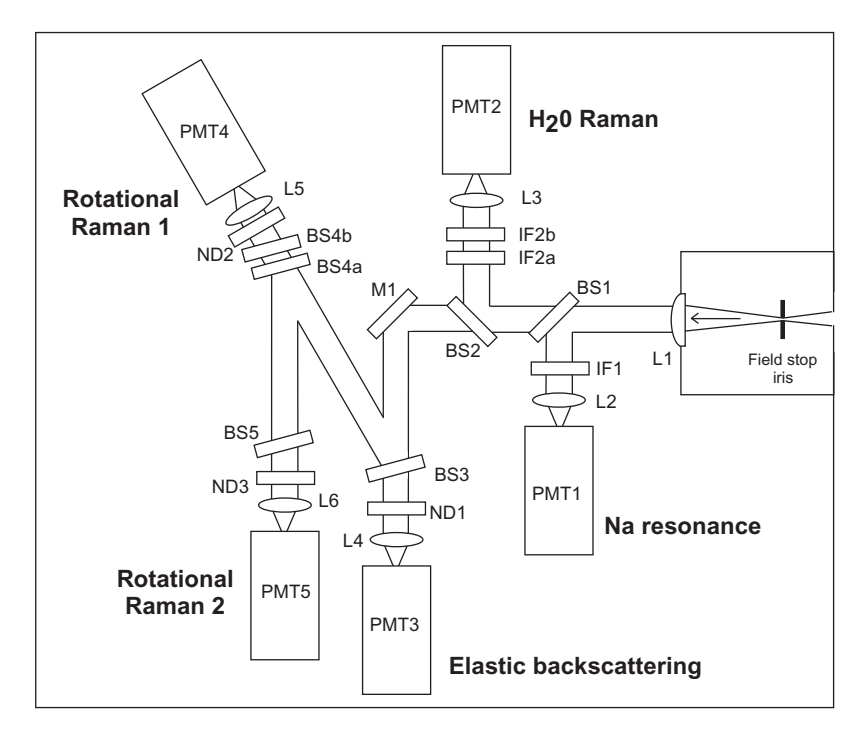


Figure 4: Schematic overview of the polychromator. L1–L6 lenses, IF1-IF2b interference filters, BS1-BS5 beamsplitters, ND1-ND3 neutral density attenuators, PMT1-PMT5 photomultiplier tubes for the signals indicated. The Na resonance channel belongs to a collocated system.

Table 2: Optical properties of the filter polychromator. AOI angle of incidence, CWL central wavelength, FWHM full width at half maximum, τ transmission, ρ reflectivity, p and s polarization parallel and perpendicular, respectively. Transmission values $\tau < 10^{-3}$ are estimations of the manufacturer.

Wavelength, nm	Parameter	BS1	BS2	BS3	BS4a & BS4b combined	BS5	IF2a & IF2b combined
	AOI,°	45	45	5.8	7.4	5.5	0
	CWL, nm			532.25	530.70	529.20	660.3
	FWHM, nm			0.74	0.55	1.20	2.6
589, s	τ						
	ρ	> 0.95					
660	τ	≈ 0.70					≈ 0.3
	ho		> 0.95				
532.11, p	τ	≈ 0.80	≈ 0.85	0.83	< 10 ⁻⁶	< 10 ⁻⁶	< 10 ⁻⁸
	ρ			0.11			
530.70	τ	≈ 0.80	≈ 0.85		0.38	< 2.10-4	
	ρ			> 0.95			
529.20	τ	≈ 0.80	≈ 0.85			0.75	
	ρ			> 0.96	> 0.96		

Table 3. Main properties of the receiving channels of the RASC lidar. CWL central wavelength, FWHM full width at half maximum, PMT photomultiplier tube

Channel	H ₂ O Raman	Elastic backscatter	Rotational Raman 1	Rotational Raman 2
CWL, nm	660.3	532.25	530.70	529.20
FWHM, nm	2.6	0.74	0.55	1.20
Polychromator transmission (entrance hole to PMT)	≈ 0.3	0.56	0.26	0.51
Total blocking at 532.11 nm	≈ 10°		≈ 10 ⁷	≈ 10 ⁷
PMT efficiency at CWL	0.13	0.13	0.13	0.13

4. MEASUREMENT EXAMPLE

First measurements with the new setup of the RASC lidar were made in May 2001. Figure 5 shows as example typical signals of the instrument taken within 9 minutes of integration time (27,000 laser shots). The rotational Raman signals though attenuated by a factor of 4 are about 2-times stronger than the signals of the GKSS Raman lidar, which were, to our best knowledge, the most intense pure-rotational Raman lidar signals before. Because of higher receiver transmittance and higher laser power of the RASC lidar (the sizes of the receiving telescopes are about the same) we expected in total an 3.5-fold increase of the intensity of the rotational Raman signals compared to the GKSS Raman lidar. With the first measurements of the RASC lidar, however, it turned out that the pure-rotational Raman signal intensities had risen by a factor of about 8. Therefore, we inserted during the measurement presented here neutral density attenuators with a transmission of 25 % in front of both rotational Raman PMTs in order to avoid both saturation of the signals in the height range of interest and the risk of signal induced noise. We explain the discrepancy of expected and actual signal intensities with losses that occur in case of the GKSS Raman lidar when the signals are coupled into a fiber. Besides allowing night time measurements with higher resolution the intensity increase leads to such high signal-to-noise values also at daylight that even daytime temperature profiling becomes feasible (see Section 5).

Figure 6 shows the temperature profile measured with the pure-rotational Raman signals. For the integration time of 9 minutes, the statistical uncertainty is only \pm 0.9 in 10 km altitude for a height resolution of 500 m. The data of the lidar and a local radiosonde agree well. In the height range of the cirrus cloud at around 11 km the first rotational Raman signal, which is closer in wavelength to the elastic signal, had to be corrected for elastic scattering leakage. Without this correction, a deviation of -5 K is seen within the cloud. The formula we applied is

$$N(z) = S(z) / [\gamma(R(z) - 1) + 1],$$

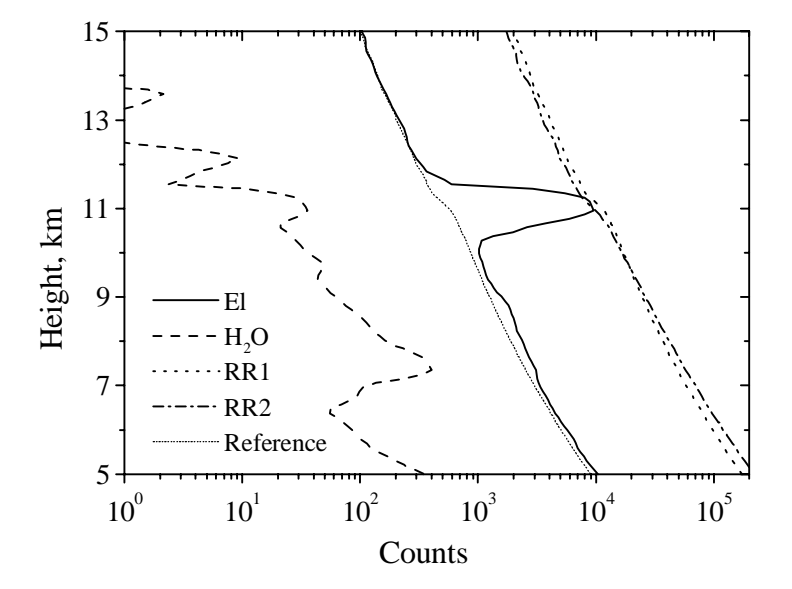


Figure 5: RASC lidar signals: elastic backscattering (solid), H_2O vibrational Raman (dashed), first pure-rotational Raman (dotted), second pure-rotational Raman (dash-dot), and temperature independent Raman reference signal derived from the pure-rotational Raman signals (short dots). The data was taken on May 16, 2001, within 9 minutes of integration time (27,000 laser shots) started at 23:28 LT. Neutral density attenuators with transmissions of 25 and 0.1 % were used for both rotational Raman channels and the elastic channel, respectively, in order to avoid PMT saturation. The rotational Raman signals were stored with a height resolution of 100 m and afterwards summed up for this plot with a 300 m gliding window length. The elastic backscattering signal and the H_2O vibrational Raman signal are shown with their raw data resolution of 300 m. The displayed data are already corrected for background noise and receiver dead-time. The reference signal was normalized at 15 km altitude to the elastic backscatter signal.

where z denotes height, z_0 a reference height without particles, S(z) the uncorrected signal, N(z) the corrected signal, γ a parameter that describes the amount of leakage, and R(z) the backscatter ratio. For the correction, $\gamma = 0.003$ was used here. With the GKSS Raman lidar, which used the same beamsplitters for the extraction of the rotational Raman signals, the measurements were unperturbed at least up to a backscatter ratio of 45. Therefore, we attribute the cloud influence on the temperature profile here to stray light inside the polychromator. With future refining of the receiver, leakage corrections should again become unnecessary.

Optical properties of a cirrus cloud, which is present in this case in the receiver field of view around 11 km height are shown in Figure 7. Maximum values of its backscatter ratio R, particle backscatter coefficient β_{par} , and particle extinction coefficient α_{par} are $R=25.9\pm0.4$, $\beta_{par}=(1182\pm5)\ 10^{-5}\ km^{-1}sr^{-1}$, and $\alpha_{par}=0.31\pm0.05\ km^{-1}$, respectively. The extinction-to-backscatter coefficient (lidar ratio) varies between 12 ± 6 and 26 ± 4 within the cloud. In modification to the mean-while common Raman technique³, we used the reference signal derived from the pure-rotational Raman signals (here, with the first rotational Raman signal corrected for elastic backscatter leakage) instead of the N_2 vibrational Raman signal to calculate these parameters (see Section 2).

The relative humidity and specific humidity profiles of this measurement example are plotted in Figure 8. Radiosonde and lidar data are in close agreement. A correction for elastic backscatter leakage had to be applied inside the cloud for the H_2O vibrational Raman signal with $\gamma = 0.03$. Because of the wavelength difference between the H_2O Raman signal at 660 nm and the reference signal at 532 nm the reference signal was modified using the known wavelength dependence of the molecular extinction coefficient of λ^{-4} .

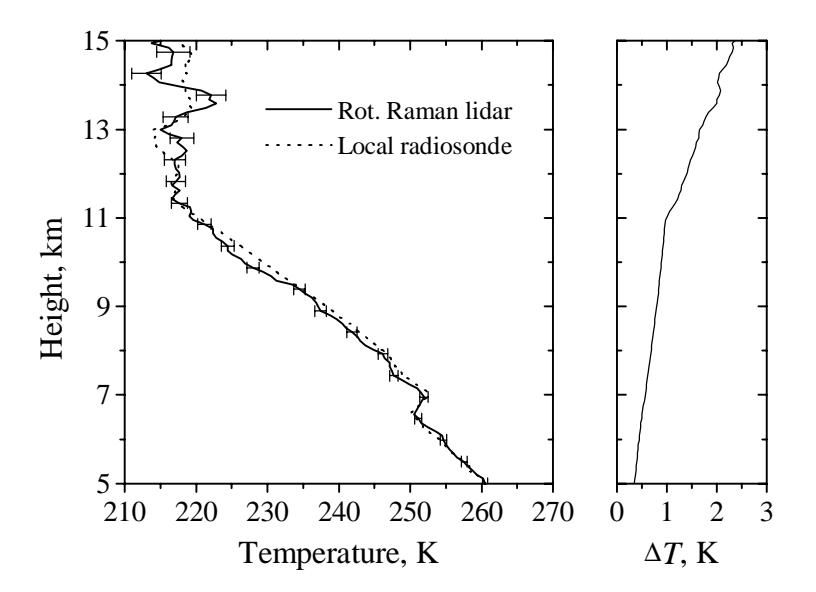


Figure 6: RASC lidar temperature measurement by rotational Raman technique (solid). The data was taken on May 16, 2001, within 9 minutes of integration time (27,000 laser shots) started at 23:28 LT (same as Fig. 5). To avoid PMT saturation the rotational Raman signal intensity was reduced to 25 % by means of neutral density attenuators. The signals were corrected for background noise, receiver dead-time, and elastic backscatter cross-talk within the cloud and averaged with a 500 m gliding window length. Error bars in the right panel and the line of the left panel show the statistical uncertainty due to signal noise. The local radiosonde (dotted) was started at the lidar site at 23:56 LT on the same day. It reached altitudes of 5, 10 and 15 km at 00:11, 00:25 and 00:39 LT, respectively. Horizontal distances at these altitudes to the lidar site were approximately 20, 60 and 120 km.

Proc. SPIE Vol. 4484

158

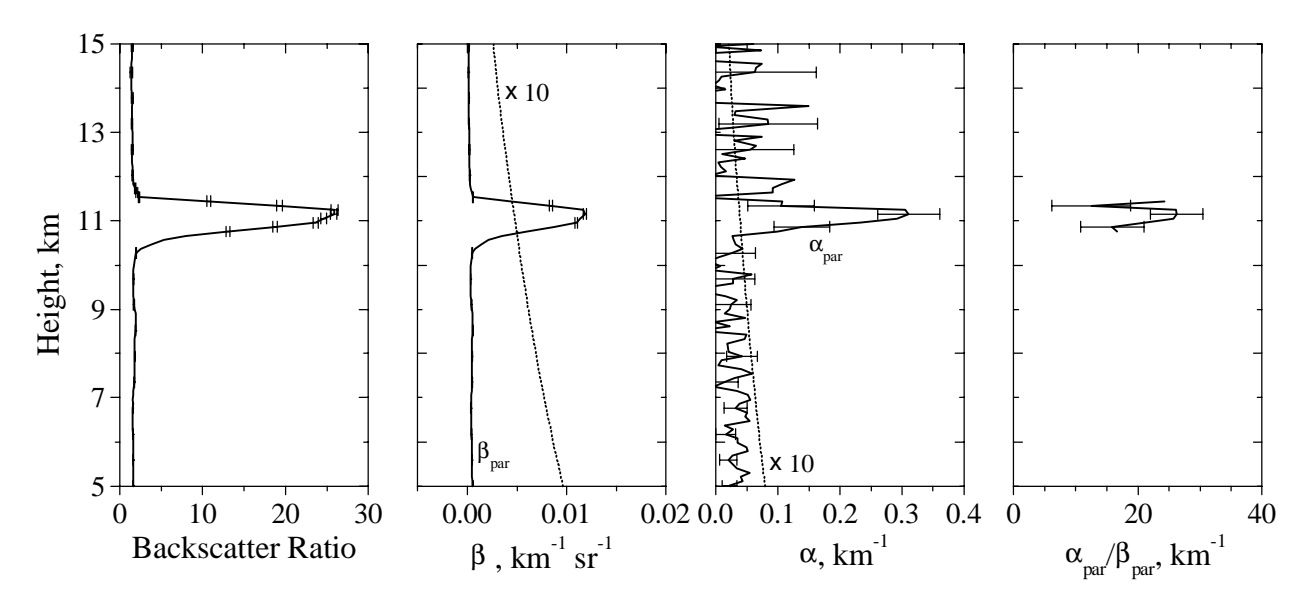


Figure 7: Backscatter ratio, particle backscatter coefficient β_{par} , particle extinction coefficient α_{par} and extinction-to-backscatter-ratio (all solid) calculated with the elastic signal and rotational Raman reference signal displayed in Figure 3. Time and height resolution are 9 minutes and 300 m, respectively. For comparison, the molecular backscatter coefficient and the molecular extinction coefficient are also shown (dotted, enlarged by a factor of 10). Error bars denote the statistical uncertainties due to signal noise.

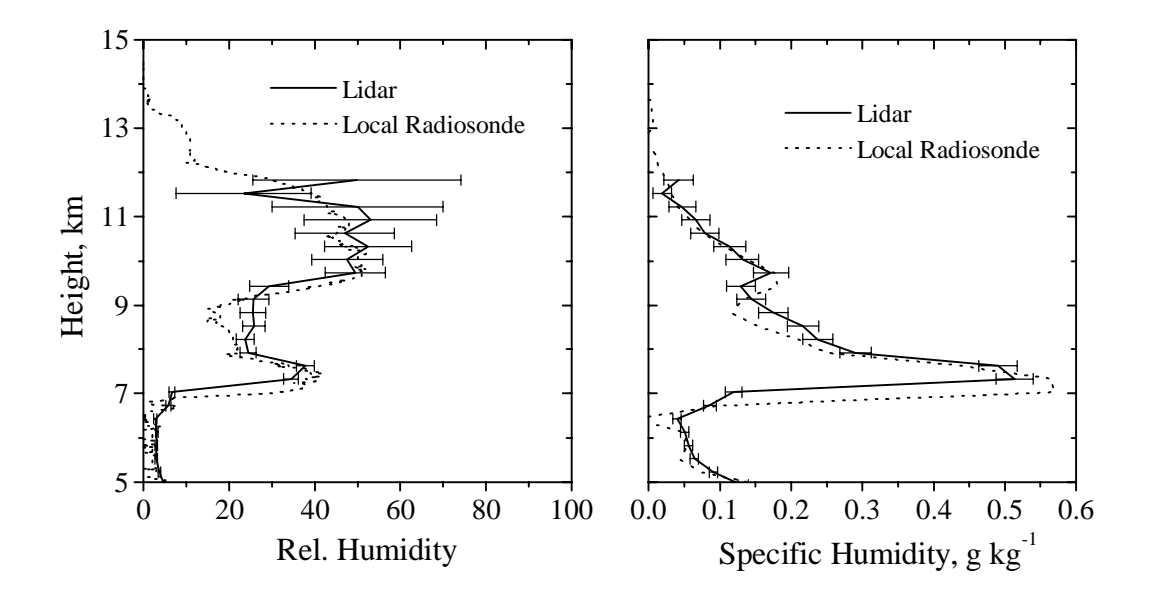


Figure 8: Relative and specific humidity derived from H_2O Raman signal and rotational Raman reference signal displayed in Fig. 3 (measurement time was 23:28 to 23:37 LT on May 16, 2001, height resolution is 300 m). Error bars show the statistical uncertainty due to signal noise. The local radiosonde (dotted) was started at 23:56 LT. It reached the altitudes of 5, 10 and 15 km at 00:11, 00:25 and 00:39 LT, respectively. Horizontal distances at these altitudes to the lidar site were approximately 20, 60 and 120 km.

5. DAYTIME ROTATIONAL RAMAN MEASUREMENTS

To realize rotational Raman lidar measurements also in daytime, it has been proposed to use a transmitter in the solar blind spectral region for lower tropospheric profiling¹⁵ or to separate single N_2 rotational Raman lines by means of Fabry-Perot interferometers¹⁶. To the authors' best knowledge, experimental results of such instruments have not been published so far. Figure 9 and Figure 10 show what is possible even without these elaborate techniques.

The temperature profile plotted in Figure 9 was taken between 8:00 and 9:01 LT on May 14, 2001, while the solar elevation angle increased from 37 to 49°. The statistical uncertainty is below ± 1 K up to a height of 7.5 km. Inversion layers, i.e., steps in the temperature profile, at about 6 and 7 km height are seen by both radiosonde and lidar. Figure 10 shows the profile at noon on the same day (solar elevation angle between 70 and 74°). Even here, the statistical uncertainty is below ± 2 K up to a height of 6.0 km. Figure 11 shows the statistical uncertainties of the temperature measurement and solar elevation angle versus local time for 3 and 5 km altitude. During the measurements no clouds were above the lidar site in the altitude range shown in Figure 9 and 10. However, haze in the boundary layer and a thin cirrus layer at about 10.5 km altitude increased solar stray light definitely above the pure Rayleigh scattering level.

The only modification of the RASC lidar from nighttime to daytime operation which we made was to change to neutral density filters with higher blocking in order to avoid saturation of the signals. Essential is a thorough correction of receiver dead-time effects as for the intensities of daytime signals the receiver response shows clear deviations from linear behavior. The relation between measured number of photons $N_{\rm m}$ and true number of photons $N_{\rm t}$ is given by

$$N_{\rm m} = N_{\rm t} \, \exp(-N_{\rm t} \, \tau)$$

with τ for the dead-time of the receiver¹⁷.

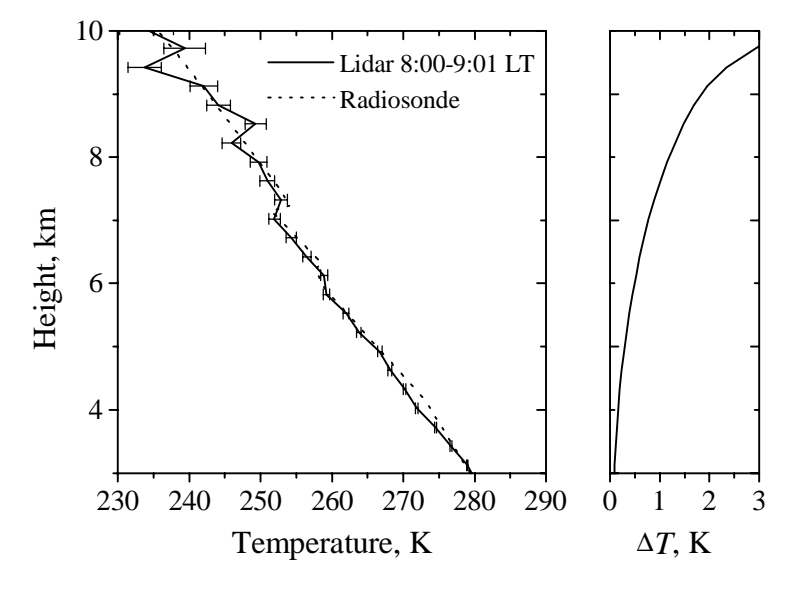


Figure 9: Daylight temperature measurement with the RASC lidar by rotational Raman technique (solid). taken between 8:00 and 9:01 LT on May 14, 2001 (1.8·10⁵ laser shots). The solar elevation angle was between 37 and 49° in this period. Neutral density attenuators with 4 % transmission were used. The rotational Raman signals were corrected for receiver dead-time and background noise and averaged with a 900 m gliding window length. Error bars in the right panel and the line of the left panel show the statistical uncertainty due to signal noise. Also shown are the temperature data of a near-by radiosonde (dotted), which was started in Shionomisaki (33.5 °N, 135.8 °E), about 150 km south of the lidar site, at 9:00 LT on the same day.

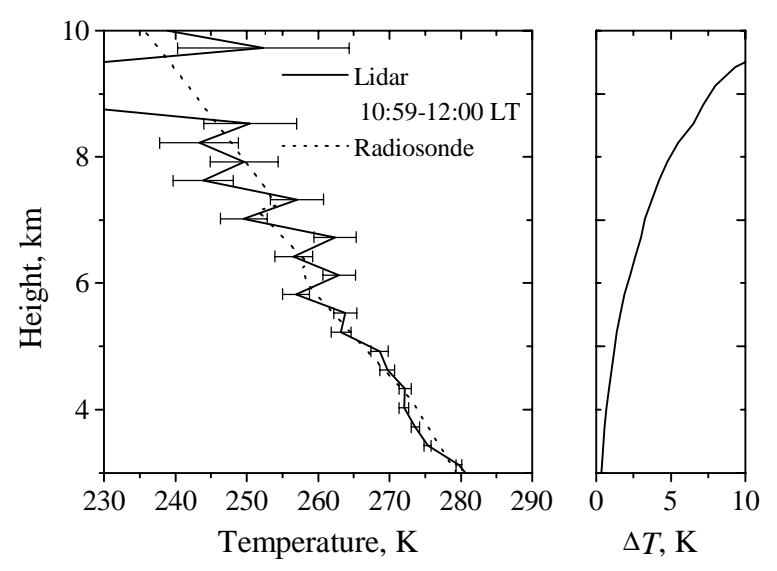


Figure 10: Same as Figure 9, but with lidar data taken between 10:59 and 12:00 LT on the same day (also $1.8 \cdot 10^5$ laser shots). The solar elevation angle was between 70 and 74°. Neutral density attenuators with 1 % transmission were used.

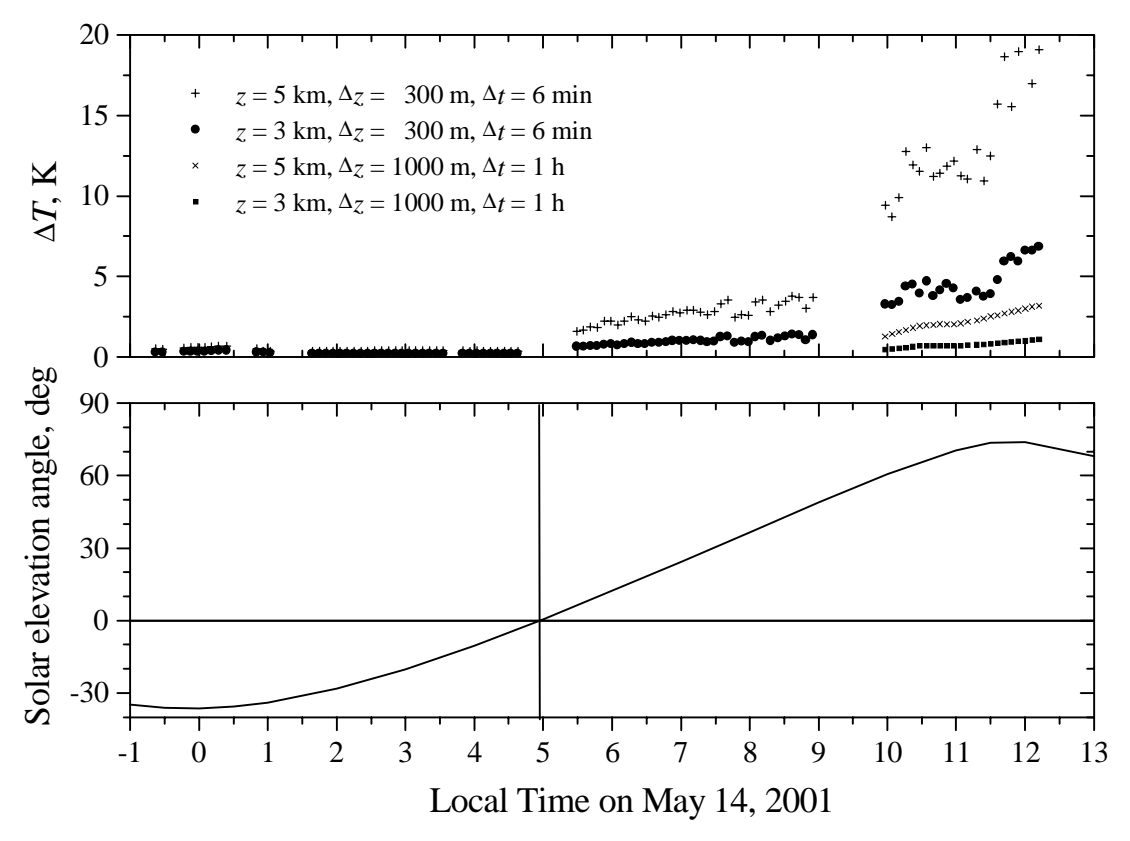


Figure 11: Statistical error of rotational Raman temperature measurements at heights z of 3 and 5 km versus local time (upper panel) and solar elevation angle in the measurement period (lower panel). For this plot the lidar data of May 13 and 14, 2001 were taken with the height and time averaging lengths indicated (Δz and Δt , respectively). Neutral density attenuators with 25, 4, and 1 % transmission were used between 23:22 and 4:38 LT, between 5:32 and 9:00 LT, and between 9:58 and 12:12 LT, respectively. The increase of the statistical temperature error displays the influence of increasing background signal.

6. SUMMARY

We introduced a novel technique for deriving a temperature independent reference signal from two pure-rotational Raman signals of different temperature dependence. The feasibility of this method was illustrated with a measurement example: Simultaneous profiles of temperature, particle extinction coefficient and particle backscatter coefficient in case of a cirrus cloud and of humidity were determined. Advantages of the new technique are both lower statistical and systematical measurement uncertainties.

The apparatus used for these measurements, the new RASC lidar, was described in detail.

The high signal-to-noise ratio of the instrument's rotational Raman signals, allowed by means of neutral density attenuators for the first time, to our knowledge, daytime rotational Raman temperature measurements.

ACKNOWLEDGMENT

Our deep gratitude is to W. Lahmann who made it possible to use the rotational Raman filters, which are owned by GKSS Forschungszentrum Geesthacht GmbH, Germany.

REFERENCES

- 1. S. Fukao, T. Sato, T. Tsuda, S. Kato, K. Wakasugi, and T. Makihira, "The MU radar with an active phased array system, 1. Antenna and power amplifiers," *Radio Sci.* 20, pp. 1155-1168, 1985.
- 2. S. Fukao, T. Tsuda, T. Kato, S. Sato, , K. Wakasugi, and T. Makihira, "The MU radar with an active phased array system, 1. In-house equipment," *Radio Sci.* 20, pp. 1169-1176, 1985.
- 3. A. Ansmann, U. Wandinger, M. Riebesell, C. Weitkamp, and W. Michaelis, "Independent measurement of extinction and backscatter profiles in cirrus clouds by using a combined Raman elastic-backscatter lidar." *Appl. Opt.* **31**, pp. 7113-7131, 1992.
- 4. J. Cooney, "Normalization of elastic lidar returns by use of Raman rotational backscatter." Appl. Opt. 14, pp. 270-271, 1975.
- 5. J. Reichardt, S. E. Bisson, S. Reichardt, C. Weitkamp, and B. Neidhart, "Rotational Vibrational Raman Differential Absorption Lidar for Atmospheric Ozone Measurements: Methodology and Experiment," *Appl. Opt.* **39**, pp. 6072-6079, 2000.
- 6. V. M. Mitev, I. V. Grogorov, V. B. Simeonov, Yu. F. Arshinov, and S. M. Bobrovnikov, "Raman lidar measurements of the atmospheric extinction profile," *Bulg. J. Phys.* **17**, pp. 67-74, 1990.
- 7. V. M. Mitev, I. V. Grogorov, and V. B. Simeonov, "Lidar measurements of aerosol extinction profiles: a comparison between two techniques Klett inversion and pure rotational Raman scattering methods." *Appl. Opt.* **31**, pp. 6469-6474, 1992.
- 8. J. Cooney, "Measurement of atmospheric temperature profiles by Raman backscatter," J. Appl. Meteorol. 11, pp. 108-112, 1972.
- 9. A. Behrendt and C. Weitkamp, "Optimizing the spectral parameters of a lidar receiver for rotational Raman temperature measurements," Proceedings of the 20th International Laser Radar Conference, 9-14 July 2000, Vichy, France, in print.
- 10. K. Kobayashi, T. Kitahara, T.D. Kawahara, Y. Saito, A. Nomura, T. Nakamura, T. Tsuda, M. Abo, C. Nagasawa, and M. Tsutsumi, "Simultaneaous measurements of the dynamical structure of the mesopause region with lidars and MU radar," *Earth Planets Space* **51**, pp. 731-739, 1999.
- 11. H. Miyagawa, T. Nakamura, T. tsuda, M. Abo, C. Nagasawa, T.D. Kawahara, K. Kobayashi, T. Kitahara, and A. Nomura, "Observations of mesospheric sporadic sodium layers with the MU radar and sodium lidars," *Earth Planets Space* **51**, pp. 785-797, 1999
- 12. A. Behrendt and J. Reichardt, "Atmospheric temperature profiling in the presence of clouds with a pure rotational Raman lidar using an interference-filter-based polychromator," *Appl. Opt.* **39**, pp. 1372-1378, 2000.
- 13. A. Behrendt, J. Reichardt, A. Dörnbrack, and C. Weitkamp, "Lidar temperature profiling in the lee of the Scandinavian mountain ridge: Investigation of polar stratospheric cloud formation conditions." Proceedings of the 19th Quadrennial Ozone Symposium, 3-8 July 2000, Sapporo, Japan, pp. 307-308, 2000.
- 14. Behrendt, A., J. Reichardt, J. Siebert, K.-H. Fricke, and C. Weitkamp, "Tropospheric and stratospheric temperature measurements by lidar above Esrange in January and February 1999." Proceedings of the Fifth European Workshop on Stratospheric Ozone, 26 September 1 October 1999, St. Jean de Luz, France, pp.153-156, 2000.
- 15. J. Zeyn, W. Lahmann, and C. Weitkamp, "Remote daytime measurements of tropospheric temperature profiles with rotational Raman lidar". *Opt. Lett.* **21**, pp. 1301-1303, 1996.
- 16. Yu. F. Arshinov, and S. M. Bobrovnikov, "Use of a Fabry Perot Interferometer to isolate pure rotational Raman spectra of diatomic molecules." *Appl. Opt.* **38**, pp. 4635-4638, 1999.
- 17. D. R. Evans, *The atomic nucleus*, p. 785, McGraw-Hill, New York, 1955.